Influence of substrates and e-beam evaporation parameters on the microstructure of nanocrystalline and epitaxially grown Ti thin films

Vivek Devulapalli, Hanna Bishara, Matteo Ghidelli, Gerhard Dehm, Christian Liebscher

Influence of e-beam evaporation parameters on the microstructure of nanocrystalline and epitaxially grown Ti thin films

Vivek Devulapalli[a], Hanna Bishara[a], Matteo Ghidelli[a,b], Gerhard Dehm[a], C.H. Liebscher[a]

[a] *Max-Planck-Institut für Eisenforschung GmbH, Max-Planck-Str. 1, D-40237 Düsseldorf, Germany*
[b] *Laboratoire des Sciences des Procédés et des Matériaux (LSPM), CNRS, Université Sorbonne Paris Nord, 93430, Villetaneuse, France*

Abstract

Titanium thin films were deposited on silicon nitride (SiN_x) coated Si, NaCl, and sapphire substrates varying the deposition conditions using e-beam evaporation to investigate thin film growth modes. The microstructure and texture evolution in dependence of substrate, deposition rate, film thickness, and substrate temperature were studied using X-ray diffraction, electron backscatter diffraction, and transmission electron microscopy. Thin films obtained on SiN_x and NaCl substrates were nanocrystalline, while the films deposited on sapphire transformed from nanocrystalline to single crystalline at deposition temperatures above 200°C. Predominantly, a surface plane orientation of (0002) was observed for the single crystalline films due to the minimization of surface energy. The orientation relationship of epitaxial single crystalline films grown on C-plane sapphire substrate is found to be $(0002)_{Ti} \parallel (0006)_{Sapphire}$, $\langle 11\bar{2}0\rangle_{Ti} \parallel \langle 03\bar{3}0\rangle_{Sapphire}$. In this orientation relationship, both the total surface and strain energy of the film are minimized. The results were complemented by resistivity measurements using the four-point probe method reporting an increase from ~60 $\mu\,\Omega$ cm to ~95 $\mu\,\Omega$ cm for single crystalline and nanocrystalline films, respectively.

1. Introduction

Titanium (Ti) is a commercially extensively used material due to its high strength to weight ratio and biocompatibility [1, 2]. Apart from its conventional bulk applications, there are emerging advancements to use it in microelectromechanical systems (MEMS) devices and hydrogen storage applications [3, 4, 5]. It is also used as an adhesive bonding layer to grow films of Pt, GaN, and Cu thin films [6, 7, 8]. These applications demand the film to have a preferred microstructure such as nanocrystallinity for high strength and fatigue resistance [9].

Nanocrystalline Ti films have been reported on NaCl [10], which is a water-soluble substrate. It is extensively used as a growth substrate or as an intermediate sacrificial film for ultra-thin metallic films. It has a wide variety of applications like transfer-printing, nanotexturing, and fabrication of metallic nanostructures for transparent flexible electrodes [11]. Likewise, due to its cubic symmetry, SiN_x is a good contender for nanocrystalline Ti films. It has massive commercial importance as a power-electronics substrate due to its high mechanical strength [12]. Furthermore, sapphire is a good choice as a substrate for depositing epitaxial thin films due to its hexagonal symmetry[13]. Epitaxy is the oriented growth of target material on top of a substrate surface. Highly epitaxial films tend towards single-crystal-like behaviour, which is of great interest especially for next-generation nano- and power electronics, optical and magnetic devices [14]. Due to the allotropic transitions, solidification from the melt-pool is not a viable way to obtain single crystalline (SC) Ti. For applications such as coating medical devices with Ti to improve their biocompatibility and wear resistance, epitaxial films to obtain a SC surface is highly attractive. Therefore, the microstructure of Ti films on all these substrates is examined in this study.

Apart from the deposition parameters, the lattice matching, symmetry of surface planes, substrate miscut, and the planes forming terraces and steps on the substrate surface [15] are variables that can alter the orientation and morphology of thin films, while maintaining substrate chemistry. The adaption of an orientation relationship (OR) between a substrate and a film is a complex phenomenon [16]. Even with a known substrate surface symmetry and chemical composition, it is in most cases not possible to predict the preferred OR [17]. Although the (0002) plane of Ti has the lowest surface energy, making it the dominant surface plane, Ti films have been reported to grow with at least six other surface plane orientations [18].

The effect of deposition parameters on Ti thin films deposited using DC sputtering have been investigated earlier, which are predominantly reported to be nanocrystalline [19, 20, 21]. However, when using e-beam evaporation a range of microstructures and orientations have been observed. For depositions made on sapphire substrate, $(10\bar{1}0)$ and $(11\bar{2}0)$ SC films were observed when deposited at a very high rate of 350 Å/s [22]. On the contrary, (0002) SC films were obtained with a growth rate of 20 Å/s [13]. 6 Å/s was stated to be the lower limit to obtain a SC film [13], but Dehm *et al.* [23] reported SC Ti at much lower deposition rates of 0.15 Å/s at substrate temperatures (T_{dep}) ranging from 373 K to 473 K for up to 100 nm thick films. Further lowering of the deposition rate to ~ 0.03 Å/s lead to a polycrystalline film with 3D island growth [24]. Interestingly, the reduction of Al_2O_3 by formation of Ti_3Al at the interface in sputter deposited Ti at room temperature (RT) with a deposition rate of 0.4 Å/s has also been reported [25]. Furthermore, with similar deposition conditions on NaCl substrates, co-existing

hcp and face-centered cubic (fcc) grains, as well as the entire film being solely nanocrystalline hcp grains, have been documented [26, 10]. Overall, these studies illustrate that a wide range of films can be obtained on sapphire and NaCl. This necessitates a thorough investigation of the effect of deposition parameters on thin film microstructure.

In this work, Ti thin films were deposited on NaCl, silicon nitride (SiN_x) on Si (100), and sapphire substrates using e-beam evaporation. The T_{dep} was varied from RT to 400°C and the growth rate was altered between 0.25 Å/s to 2.5 Å/s. The film thicknesses were on the order of 100 – 300 nm. The microstructure and OR between the film and substrate were studied using electron backscatter diffraction (EBSD) and transmission electron microscopy (TEM). The first section presents the textured nanocrystalline films obtained on SiN_x and NaCl substrates, followed by details of single-crystalline films obtained on sapphire. The role of the substrate on the resulting microstructures and ORs is discussed. Electrical resistivity measurements indicated a limited change of resistivity within the SC films based on their thickness but a steep increase in the nanocrystalline film.

2. Experimental

Ti pellets (99.995%, 1/4"*dia.*) were purchased from Kurt J. Lesker Company to be used as the target. The films were deposited in a BesTeck PVD cluster (MPIE, Düsseldorf) on NaCl (100), SiN_x on silicon (100) and sapphire C-plane (0002), C-plane with a 2° miscut along [11$\bar{2}$0], sapphire A-plane (11$\bar{2}$0) and R-plane (1$\bar{1}$02) substrates. The deposition conditions are listed in Table 1. SiN_x and sapphire substrates were obtained from Siegert Wafer GmbH. In the SiN_x substrate, the 50 nm nitride layer on the Si (100) substrate acts as a diffusion barrier and prevents the reduction of Si with Ti at higher temperatures. The SiN_x substrate was heated to 500°C for 30 min before the deposition to clear off adsorbates and improve film adhesion. The substrate was then cooled down to 200°C for deposition. The NaCl substrate was cleaved in air right before the deposition to obtain clean (100) surface planes. Sapphire wafers were one side epi-polished having a surface roughness of ≤ 0.3 nm. These substrates were used in the as-received state with no additional surface treatments required. **The deposition chamber was pumped down to 2×10^{-8} mbar for all the depositions.** The substrate to target distance was ~250 mm. The e-beam current was tuned to the values ranging from 50 to 150 mA which was calibrated using a quartz microbalance and constantly monitored during the deposition. To double-check the calibration, the actual deposition rate was calculated post-deposition using film thickness and deposition duration.

First, the surface of the deposited films was subsequently examined by using a Zeiss Axio Imager light optical microscope (LOM) to detect cracks or other visible defects. The global film microstructure was determined by X-ray diffraction (XRD) using a Seifert ID3003 diffractometer equipped with a Huber 4 circle goniometer using Cu–Kα (λ = 1.54Å) and Co–Kα (λ = 1.78Å) radiation and a scintillation detector to verify the purity of the films and to measure the macro-texture. XRD was performed for a 2θ range of 30 to 90° with a point focused beam of 1 × 3 mm diameter. Grazing incidence XRD (GIXRD) was used with a 1°-incidence angle to avoid diffraction from the single crystal substrates.

The local surface morphology and film orientation was determined by scanning electron microscopy (SEM) and EBSD in a Thermo Fisher Scientific Scios2HiVac dual-beam SEM. For films deposited on NaCl substrate, the substrate was dissolved in distilled water and then picked up using 3 mm diameter molybdenum TEM grids. The grids containing the film can be directly placed inside the TEM holder after drying for several hours in the air. For films deposited on sapphire, a standard lift-out technique in a focused ion beam (FIB) instrument (Scios2HiVac) with Ga^+-ion source was used to extract TEM lamella of <100 nm thickness. The beam current was gradually reduced in several steps starting from 1 nA at 30 kV for coarse milling to eventually 27 pA at 2 kV for final polishing. All TEM work was done using an image aberration-corrected Titan Themis 80-300 (Thermo Fischer Scientific) TEM. Selected area diffraction patterns (SADP) were obtained by inserting a 10 μm aperture. High-resolution transmission electron microscopy (HRTEM) observations were done under negative C_s (-10 μm) conditions using an accelerating voltage of 300 kV.

The electrical resistivity of the thin films was determined by adapting the Van der Pauw method [27] on 1 cm × 1 cm pieces cut from the wafer after deposition. Four contacts were positioned on the top surface close to the corners of the sample using a LINKAM HFS-600 system. A direct current (DC) of 0.01 A is applied by a current generator (Keithly 6221) in the form of 10 ms pulses. The consequent voltage is measured at half-time of the pulse duration employing a voltmeter (Keithly 2182A). A series of 200 pulses are applied for increased accuracy.

3. Results and Discussion

3.1. Deposition on SiN_x and NaCl

At a deposition rate of 2.5 Å/s, a 75 nm thick Ti film was deposited on SiN_x substrate heated to 200°C. According to LOM, a smooth surface with no visible cracks or porosity was obtained (Sup. Fig. 1). The polycrystalline nature of the film is revealed by the presence of all diffraction planes in the GIXRD data shown in red in Fig. 1. From the full width at half maximum (FWHM) of the most intense Ti peak and using the Scherrer equation [28], the average crystallite size was estimated to be 20 to 30 nm along the surface normal direction. The peaks were symmetrical with the 2θ peak positions coinciding with that of bulk α-Ti [29], which indicates that global residual stresses in the film are negligible. However, a preferred (10$\bar{1}$0) texture was observed.

To explain the observed texture, the total free energy of a thin film can be calculated by the sum of the surface and strain energy [30] which the system tries to minimize during deposition. The surface energy is determined by the coordination number or atomic density of the respective lattice planes. In Ti, the (0002) plane has the lowest surface energy (2.8 J/m^2),

Table 1: List of deposited films using e-beam deposition with their deposition parameters.

Sample No.	Substrate	Deposition temperature (°C)	Thickness (nm)	Rate (Å/s)	Microstructure
Si1	Si_3N_4 (100) (50 nm)	200°C	75	2.5	NC
N1	NaCl (100)	RT	90	0.25	NC
N2	NaCl (100)	RT	90	0.8	NC
N3	NaCl (100)	200°C	75	2.5	NC
S1	Sapphire – C-plane (0001)	RT	200	0.5	SC
S2*	Sapphire – C-plane (0001)	300°C	200	0.7	SC
S3	Sapphire – C-plane (0001)	RT	90	2.5	SC
S4	Sapphire – c-2° miscut	RT	90	2.5	NC
S5	Sapphire – A-plane (11$\bar{2}$0)	RT	90	2.5	NC
S6	Sapphire – R-plane (1$\bar{1}$02)	RT	90	2.5	NC
S7	Sapphire – C-plane (0001)	200°C	300	2.5	SC
S8	Sapphire – c-2° miscut	200°C	300	2.5	SC
S9	Sapphire – A-plane (11$\bar{2}$0)	200°C	300	2.5	SC
S10	Sapphire – R-plane (1$\bar{1}$02)	200°C	300	2.5	NC
S11	Sapphire – C-plane (0001)	400°C	300	2.5	SC
S12	Sapphire – c-2° miscut	400°C	300	2.5	SC
S13	Sapphire – A-plane (11$\bar{2}$0)	400°C	300	2.5	SC
S14	Sapphire – R-plane (1$\bar{1}$02)	400°C	300	2.5	SC

RT – Room temperature, NC – Nanocrystalline, SC – Single-crystalline, * - Deposited using Ar-ion sputtering,

followed by (10$\bar{1}$0) and (10$\bar{1}$1) (3.7 J/m^2). Detailed thermodynamic calculations of the surface energy using their planar densities have been reported earlier [18, 31]. The strain energy, on the other hand, is defined by the film's strain and the anisotropy of elastic modulus [18]. The elastic anisotropy of Ti results in a 30% lower elastic modulus for the [10$\bar{1}$0] than the [0002] direction [18]. As a result, a competing growth of these three planes is observed, resulting in the film's overall free energy being minimized [17]. The lower strain energy of the (10$\bar{1}$0) orientation seems to be responsible for the observed texture in the film grown on SiN_x.

The film deposited on NaCl (100) under the same conditions (T_{dep} = 200°C, Rate = 2.5 Å/s, thickness = 75 nm), was observed using LOM to be severely buckled (Sup. Fig. 2), indicating large residual compressive stresses in the film. The thermal expansion coefficient of NaCl is an order of magnitude higher than Ti [32], which promotes the evolution of large compressive stresses in the film upon cooling from T_{dep} to RT leading to buckling. **The GIXRD pattern shown in Fig. 1 confirms the polycrystalline nature of the film albeit with a (10$\bar{1}$1) texture. The revealed texture matches well with that observed by Campbell *et al.* [26]. This can be explained by the relatively low surface energy of the (10$\bar{1}$1) plane, as discussed above, making it one of the favoured surface normal planes.** In addition, the (10$\bar{1}$1) orientation leads to lower lattice misfit than (0002) orientation. NaCl has a lattice constant of 5.64 Å, and the Ti (10$\bar{1}$1) plane has a cell size of 2.95 × 10.66 Å^2. Simply based on the geometry, the misfit between the film and substrate can be calculated by superimposing the Ti (10$\bar{1}$1) plane on the NaCl (100) plane. The OR leading to the lowest misfit can hence be calculated as:

$$\delta = (1 - \frac{d_f}{d_s}) \quad (1)$$

where d_s is the lattice spacing of the substrate, d_f the lattice spacing of the film plane. The lowest misfit of 5.49 % is achieved for $(10\bar{1}1)_{Ti} \parallel (001)_{NaCl}$ when using the domain matching epitaxy (DME) [33] with a 1/2 domain matching between Ti and NaCl. This describes the (10$\bar{1}$1) texture that is observed.

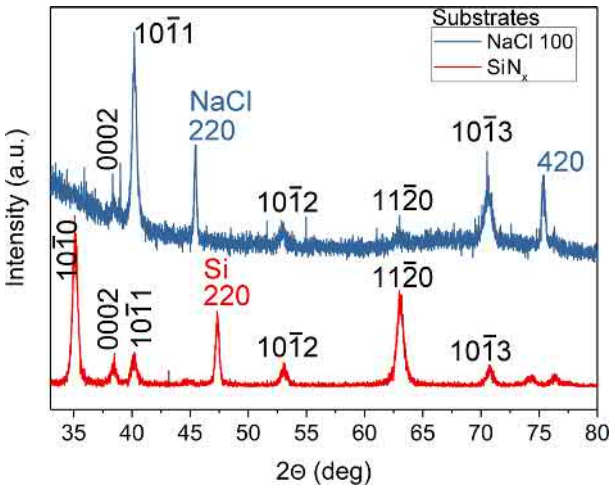

Figure 1: Grazing-Incidence XRD (Cu-Kα source) of a 75 nm thick Ti thin film deposited at 200°C on SiN_x (100) (sample #Si1) and NaCl (100) (sample #N3). Both films exhibit a polycrystalline microstructure. The film deposited on SiN_x shows a strong (10$\bar{1}$0) texture; the film grown on NaCl a (10$\bar{1}$1) texture.

In Fig. 2a, the cross-sectional bright-field TEM (BF-TEM) image of the film grown on SiN_x substrate confirms the nanocrystalline microstructure and the absence of any reaction between the film and the substrate. The grain size of 20 ± 5 nm is in the same range as estimated from the XRD data above. The corresponding diffraction pattern shown in Fig. 2b also verifies the

film's nanocrystalinity and hcp crystal structure.

Furthermore, for all films grown on NaCl, TEM was used to examine the nanocrystalline grain structure and to determine the impact of deposition rate and T_{dep} on the film microstructure. Fig. 2c shows a representative plane view BF-TEM image of sample #N1 (nanocrystalline film on NaCl at RT; deposition rate = 0.25 The grain size was measured by the line intercept method [34] to be ~54 ± 13 nm. The film adopts the α-Ti (hcp) structure as verified from the diffraction rings in Fig. 2d. **Although the film produced ring patterns, a preferred $(10\bar{1}1)$ texture is observed, which is identical to what the XRD revealed above. The surface diffusivity of condensing Ti atoms on the substrate surface is considerably lower at RT compared to elevated temperatures. According to the structural zone model, the lack of sufficient thermal energy to activate surface diffusion of adatoms results in the formation of nanocrystalline grains at RT [35].**

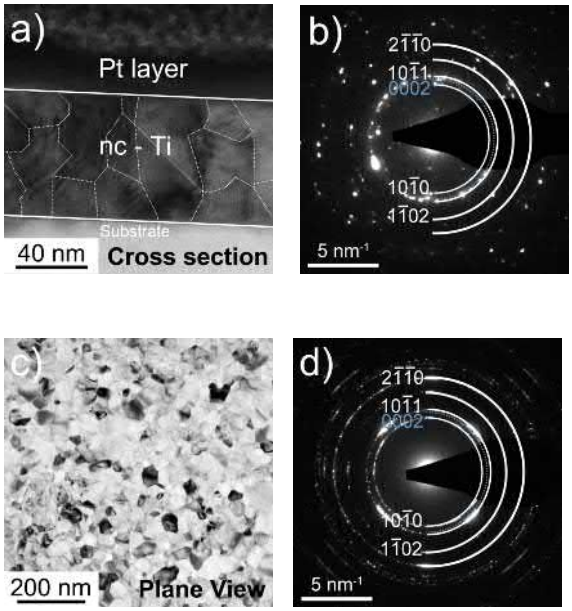

Figure 2: TEM bright field image showing the microstructure of the Ti thin film deposited (a) at 200° C on SiN_x substrate (cross section, sample #Si1) and (c) at RT on NaCl (100) substrate (plane view, sample #N1), with respective selected area diffraction patterns in (b) and (d) verifying the nanocrystalline hcp α-Ti structure.

The BF-TEM images shown in Fig. 3a and Fig. 3c are taken from sample #N2 on NaCl (100) at RT; deposition rate = 0.8 Å/s) and sample #N3 on NaCl (100) at 200°C; deposition rate = 2.5 Å/s) respectively. The average grain size of both films was determined to be ~31 ± 10 nm and ~53 ± 18 nm, as shown in Table 2. The grain size decreases from 54 ± 13 nm in #N1 to 31 ± 10 nm in #N2 with increasing deposition rate, both at RT. The smaller grain size stems from the increase in nucleation rate. The increased nucleation events are a direct consequence of the lower mean free path due to the higher flux of adatoms at higher deposition rates. This observation is contrary to the general observation that an increase in deposition rate increases grain size [36]. The latter is valid only at higher deposition temperatures when growth is not limited by surface diffusion [37]. Because these depositions were performed at RT, surface diffusion is severely limited. On the other hand, for sample #N3 (Fig. 3c), the deposition temperature was increased from RT to 200°C. The increase in substrate temperature results in a higher surface diffusivity leading to larger grain size. Assuming that the cleaved NaCl substrate surface played an identical role in the film growth in all cases, the observations indicate that lowering the deposition rate at RT and increasing the deposition rate at higher temperatures leads to an increase in grain size for NaCl (100) substrate.

Table 2: Grain size distribution of Ti thin films deposited on NaCl (100) by varying substrate temperature and deposition rate

Film	T_{dep} (°C)	Rate (Å/s)	Grain size (nm)
Si1	200°C	2.5	20 ± 5
N1	RT	0.2	54 ± 13
N2	RT	0.8	31 ± 10
N3	200°C	2.5	53 ± 18

The corresponding SADPs shown in Fig. 3b and Fig. 3d confirm the nanocrystalline nature of the films. The intensity of diffraction spots is restricted to only certain orientations going from film #N1 to #N3 as seen in Fig. 2d, Fig. 3b and Fig. 3d, respectively. Hence, an increasing degree of $(10\bar{1}1)$ texture is observed on increasing both deposition rate and T_{dep}.

It is known that water is adsorbed on the surface of alkali halides [38]. Based on the humidity of the environment the (100) surface of NaCl is most likely covered with 0.5 monolayer of water at RT. Thus, the surface partly resembles an amorphous state [39]. For amorphous substrates, the surface energy γ_i is not expected to change with the in-plane rotation, which results in an equal probability of grains with all possible in-plane rotations to grow [40]. **Since the substrate was cleaved in air in our experiments, we can conclude that water is physisorbed on its surface and the polycrystalline film deposited on NaCl at RT should exhibit all in-plane rotations. However, the minimization of surface and interface energy during the pre-coalescence stage of the film growth plays a major role in deciding the texture of the film [40].** Hence, a weak $(10\bar{1}1)$ texture is observed in Fig. 2d. In film #N2, the increased deposition rate leads to preferred growth of low energy planes promoting the $(10\bar{1}1)$ texture. Once the deposition temperature is raised, the physisorbed water layer evaporates from the NaCl surface. Hence, in film #N3, where the substrate was heated to 200°C during deposition, the surface anisotropy of NaCl comes into play leading to a much stronger $(10\bar{1}1)$ texture. This exhibits the control in microstructure that is made available by alteration of the deposition parameters. **All the four films discussed in the preceding section are nanocrystalline. As a result, these findings pave the way for better-informed deposition of nanocrystalline Ti, which is known for its exciting properties such as high strength**

and corrosion resistance [41].

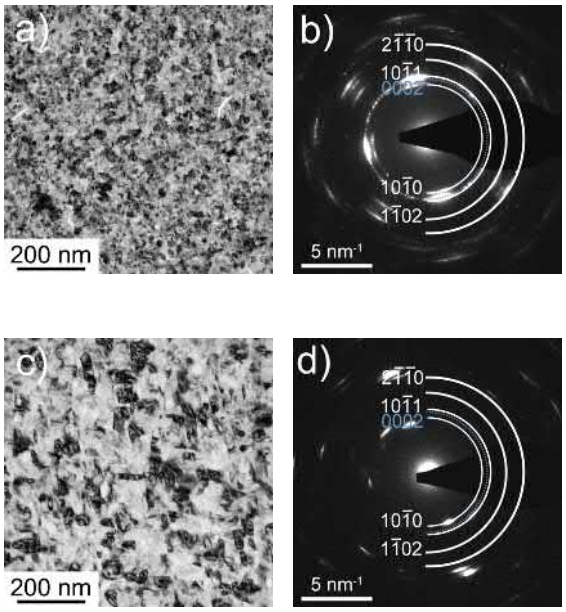

Figure 3: Plane view TEM bright field image of a Ti thin film deposited at (a) 0.8 Å/s deposition rate at RT (sample #N2) and (b) 2.5 Å/s deposition rate at 200°C on NaCl(100) substrate (sample N3). The corresponding selected area diffraction patterns are shown in (b) and (d), respectively, both exhibiting a strong $(10\bar{1}1)$ texture.

3.2. Deposition on sapphire substrate

Apart from the commercial importance due to its atomically flat and chemically inert surface, sapphire represents an excellent template for understanding the influence of substrate on thin film growth. As shown in the Fig. 4a, the GIXRD patterns of Ti deposited on C-plane sapphire (0001) at RT resulted in only a (0002) peak. The film grew as a SC, which means that there was only one orientation present across the entire two-inch wafer. The (0002) plane grows parallel to the c-axis of the substrate to minimize the surface energy. Although there is a large misfit of 7.5% between Ti and C-plane sapphire, an apparent six-fold symmetry of the oxygen-terminated sapphire surface allows the first monolayer of Ti to conform to the oxygen sub-lattice. This reduces the mismatch and allows for epitaxial growth [42].

Ti films were also deposited at RT on other configurations and orientations of sapphire like C-plane with a 2° miscut (C_{2mis}) along the $[11\bar{2}0]$ direction, the A-plane $(10\bar{1}0)$ and the R-plane $(1\bar{1}02)$. The GIXRD patterns of these films led to multiple diffraction peaks, indicating the growth of polycrystalline films. The varying degree of texture based on the substrate orientation can be seen in Fig. 4b. The sapphire substrate surface with a miscut is not atomically flat unless annealed [43]. Hence, the defects on the substrate surface lead to films having no preferential orientation during nucleation. The limited adatom mobility at RT promotes poly-/nanocrystalline film. Hence, a 2° miscut was seen to be sufficient to modify film growth from SC to poly-/nanocrystalline as has been reported in several other materials grown on sapphire [43, 44]. However, a (0002) texture is observed in all three cases similar to the C-plane substrate which can be explained by its low surface energy.

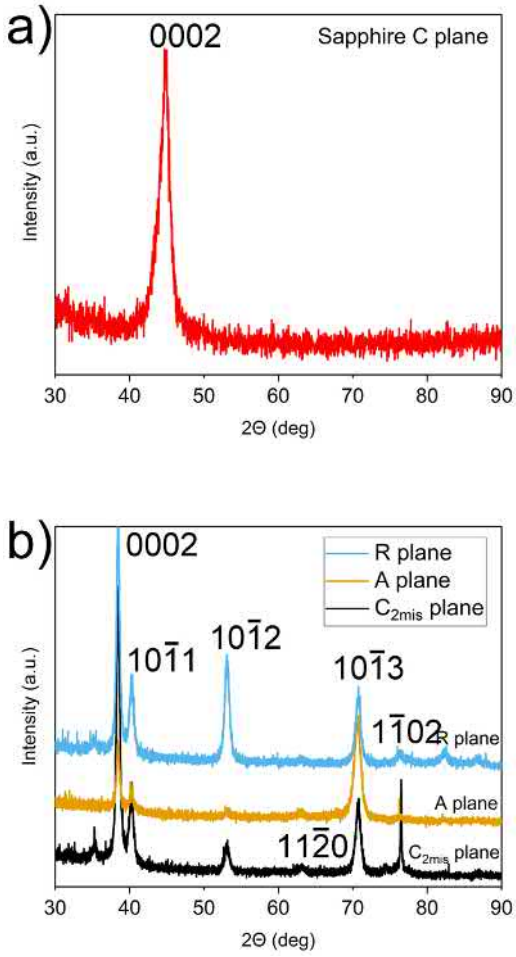

Figure 4: Grazing-Incidence XRD of 90 nm thick Ti thin films deposited at RT on (a) C-plane sapphire with only the (0002) peak present (Co-Kα source), (b) C-plane with a 2° miscut(C_{2mis}), A-plane and R-plane sapphire displaying multiple diffraction peaks (Cu-Kα source)

Further batches of depositions using the same set of sapphire substrates were performed at higher deposition temperatures to study the influence of T_{dep} on film microstructure. The deposition on C-plane sapphire, C_{2mis} and A-plane at 200°C (samples #S7, #S8 and #S9) resulted in highly epitaxial single-crystalline films. They were deposited after holding the substrates at T_{dep} for ∼1 h to ensure uniform temperature. The holding period results in desorption of water and any organic/volatile impurities from the substrate surface. An epi-polished sapphire substrate surface is known to exhibit surface steps [45]. Additionally, the increase of T_{dep} results in an increased surface diffusion of adatoms. The islands which nucleate on the atomic steps in the C_{2mis} substrate are hence expected to have fixed orientation relationship with surface steps and better interconnections between neighboring grains at higher T_{dep}, which leads to a single dominant orientation [43]. A similar effect is

observed in A-plane sapphire which leads to the ease of SC film formation. However, the film remained polycrystalline for the R-plane sapphire substrate at 200°C.

There are three ways epitaxial films deposited on sapphire substrates can grow. When the bond between the adatom and the substrate is strong, a layer-by-layer deposition called Frank-van der Merwe (FM) mode can occur [46]. The Volmer-Weber (VW) growth mode is caused by a stronger bond between the adatoms, resulting in their three-dimensional clusters to coalesce and form a continuous film. A combination of the two, where clusters form on top of a few monolayers is termed Stranski–Krastanov (SK) growth mode [46]. Which of these growth modes is dominant is determined by the rivalry between the bare substrate's surface energy (γ_{sv}), the interface energy between the substrate-film (γ_{sf}), and between the film-vapor (γ_{fv}). A large misfit system like in the above films leads to a high γ_{sf} value, which results in a significantly lower barrier to nucleate clusters, favouring the VW growth mode. As a result of the formation of several tiny nuclei at RT, a nanocrystalline film was found in all but one of the cases. The only exception was C-plane sapphire, which was SC as previously discussed.

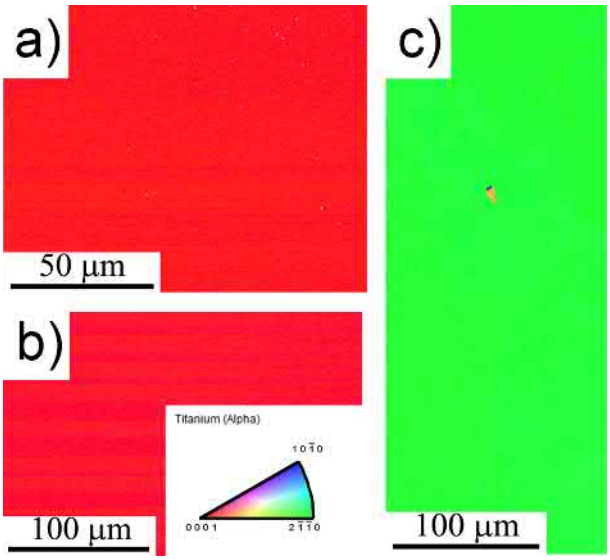

Figure 5: Inverse pole figure (IPF) obtained from EBSD of Ti thin films deposited at 400°C on (a) C_{2mis}-plane (b) A-plane and (c) R-plane sapphire at low magnification to display uniform orientation over the entire wafer.

To verify the observations and to explain the anomalous behaviour of R-plane sapphire, the substrate temperature was further increased to 400°C. This leads to a further increased mobility of adatoms resulting in SC film formation on all the sapphire substrate orientations (samples #S11, #S12, #S13 and #S14). EBSD scans of the film surfaces revealed no change in orientation. The scans were observed in both transverse and planar viewing direction using TSL-OIM software to confirm the absence of grain boundaries even with a 1° angular deviation. The film deposited on C-plane (not shown), C_{2mis} and A-plane all demonstrated the same preferred $(0002)_{Ti}$ orientation as shown in Fig. 5 a and b. The orientation of the film on C-plane and

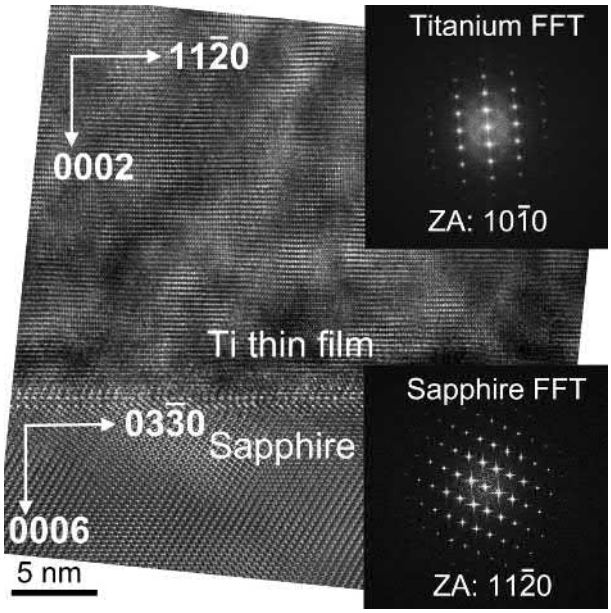

Figure 6: HRTEM image of cross-section of Ti thin film deposited on C-plane sapphire shows a 90 nm thick Ti film deposited using e-beam evaporation at RT (sample #S3) observed in [11$\bar{2}$0] zone axis orientation of the sapphire substrate. The insets show fast Fourier transforms (FFTs) of the film and substrate, respectively, which are used to determine the ORs

C_{2mis} can be explained in the same way as in the previous two cases. A-plane sapphire has a two-fold symmetry with [0001] perpendicular to [1$\bar{1}$00] results in a super-cell of 12.99 Å × 8.22 Å. When depositing Ti on this plane at sufficiently high temperature (here 200°C), the favoured out-of-plane OR is observed to be $(0002)_{Ti} \parallel (\bar{1}\bar{1}20)_{Sapphire}$ [47]. However a 30° in-plane rotation separates the two ORs. The $\langle 10\bar{1}0\rangle_{Ti} \parallel \langle 1\bar{1}00\rangle_{Sapphire}$ results in 18.01% and 7.6% misfit in [0001] and [10$\bar{1}$0] directions respectively, whereas, in the same directions $\langle 11\bar{2}0\rangle_{Ti} \parallel \langle 1\bar{1}00\rangle_{Sapphire}$ results in a misfit of 9.16% and 24.33%, respectively. Due to the relatively lower misfit, the former is observed here. The SC film on R-plane sapphire exhibited a $(2\bar{1}\bar{1}0)_{Ti}$ surface plane normal, which is reported here for the first time.

Unless the in-plane orientation of the underlying substrate is known, observing the film surface using EBSD is insufficient to find the OR. Hence, high resolution-TEM (HRTEM) of the interface viewed in cross-section was used to observe the OR between the SC film and the C-plane sapphire substrate in the sample #S3 (deposited using e-beam evaporation at RT). As shown in Fig. 6, accommodating a 7.58% misfit [48], the film was found to have $(0002)_{Ti} \parallel (0006)_{Sapphire}$, $\langle 11\bar{2}0\rangle_{Ti} \parallel \langle 03\bar{3}0\rangle_{Sapphire}$ OR in agreement with [23]. Sup. Fig. 3 shows the sample #S2 deposited with Ar–ion sputtering at 200°C exhibits the same OR. This demonstrates that the OR between Ti and sapphire C-plane is independent of the deposition method.

3.3. Resistivity measurements

Ti thin films can be used in micro-electronic miniaturised circuits, electrical contacts and sputter ion pumps. These applications require a control of the electrical resistivity of the thin films. Based on the thickness, deposition parameters, chemical

purity of the target and microstructure of the film, the resistivity values can largely vary [49]. **As seen in the Fig. 7, for the films deposited on C-plane sapphire, the thinner film (sample #S3), with thickness of 90 nm, shows a higher resistivity of ~70 $\mu\ \Omega$ cm. This increased resistivity can be attributed to increased surface scattering. For the 300 nm thick SC films (sample #S7 and #S11) resistivity remains uniform at ~60 $\mu\ \Omega$ cm, which is slightly higher than the pure bulk single crystal values of Ti (~40 $\mu\ \Omega$ cm) [50, 22] which can also be attributed to surface scattering. The values measured here are in agreement with other epitaxial Ti films [22], and are much lower than the polycrystalline films reported in literature [51, 50, 52].** Apart from the surfaces, grain boundaries can also act as scattering centers. Resulting from increased scattering from grain boundaries, the nanocrystalline film grown on sapphire A-plane at RT (sample S5) exhibited a much higher resistivity of ~95 $\mu\ \Omega$ cm, while the thicker films on A-plane sapphire show the same trend as seen for C-plane. As suggested by Bel'skaya *et al.* [53], the resistivity values of thin films can also be used as a measure of the impurity content, given the deposition conditions are same. Hence, the resistivity of ~60 $\mu\ \Omega$ cm in the SC films indicates that impurities play a minor role on resistivity.

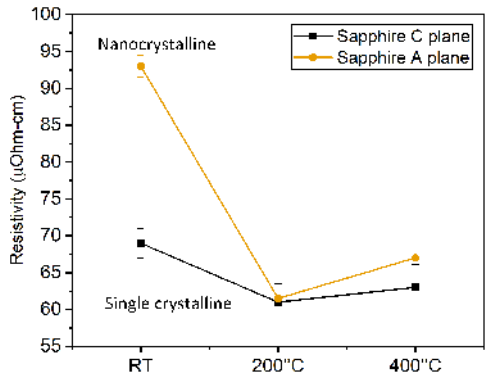

Figure 7: Resistivity values of films grown on C-plane sapphire and A-plane at varying T_{dep}. The only nanocrystalline film shows higher resistivity of ~ 95 $\mu\ \Omega$ cm while all SC films show resistivity of ~ 60 $\mu\ \Omega$ cm

4. Conclusion

In this study titanium thin films were successfully deposited using e-beam evaporation on substrates of SiN_x, NaCl and four orientations of sapphire. The substrate temperature and deposition rate were varied in order to study their influence on microstructure and texture.

1. **Nanocrystalline films were obtained for the first time on SiN_x. All depositions on NaCl substrate also led to nanocrystalline films. However, a difference in texture between the two was observed. The minimization of strain energy dominated for the film deposited on SiN_x substrate leads to a $(10\bar{1}1)$ texture, while surface energy minimization promotes a $(10\bar{1}0)$ texture of all films deposited on NaCl (100). An increase of deposition rate resulted in a minor increase in the grain size. Nevertheless, all the films were nanocrystalline, which can be of great commercial interest for applications requiring high strength and corrosion resistance.**
2. The film on C-plane sapphire grew as a single crystal with (0002) plane surface normal in all cases. The six-fold symmetry of the oxygen sub-lattice of sapphire and the low lattice misfit are considered to be responsible for the formation of a SC film even at RT. Using cross-section HRTEM imaging the orientation relationship was determined to be $(0002)_{Ti} \parallel (0006)_{Sapphire}$, $\langle 11\bar{2}0\rangle_{Ti} \parallel \langle 03\bar{3}0\rangle_{Sapphire}$.
3. **On C-plane sapphire with a 2° miscut and A-plane, a nanocrystalline film grew at RT and SC films were obtained by heating the substrate to 200°C. For the first time, a SC film was obtained on R-plane sapphire by heating the substrate to 400°C.**
4. The resistivity of the 90 nm thick SC film was 70 $\mu\ \Omega$ cm while 300 nm thick films displayed lower resistivity of 60 $\mu\ \Omega$ cm owing to reduced surface scattering with increasing film thickness. The nanocrystalline film exhibited higher resistivity of 95 $\mu\ \Omega$ cm because of additional scattering from grain boundaries.

These results pave the way to a controlled synthesis of Ti films with defined orientations having fundamental implications for micro-electronics and thin film industry.

5. Acknowledgement

VD and CHL acknowledge funding from the KSB Stifftung. HB and GD acknowledge funding from the European Research Council (Grant no. 787446-GB-CORRELATE). The authors would like to thank Mr. Benjamin Breitbach for conducting the X-ray diffraction experiments. The assistance of Mr. Dennis Klapproth and Mr. Andrea Brognara during film deposition is also gratefully acknowledged.

References

[1] D. Banerjee, J. Williams, Perspectives on Titanium Science and Technology, Acta Materialia 61 (2013) 844–879.
[2] R. Van Noort, Titanium: The implant material of today, Journal of Materials Science 22 (1987) 3801–3811.
[3] Z. Tarnawski, N.-T. T. Kim-Ngan, Hydrogen storage characteristics of Ti– and V–based thin films, Journal of Science: Advanced Materials and Devices 1 (2016) 141–146.
[4] K. Hofmann, B. Spangenberg, M. Luysberg, H. Kurz, Properties of evaporated titanium thin films and their possible application in single electron devices, Thin Solid Films 436 (2003) 168–174.
[5] I. Gablech, O. Caha, V. Svatoš, J. Pekárek, P. Neužil, T. Šikola, Stress-free deposition of [001] preferentially oriented titanium thin film by Kaufman ion-beam source, Thin Solid Films 638 (2017) 57–62.
[6] J.-N. Aoh, C.-L. Chuang, Thermosonic Bonding of Gold Wire onto a Copper Pad with Titanium Thin-Film Deposition, Journal of electronic materials 33 (2004) 290–299.

[7] J. Yu, J. Wang, B. Lu, Y. Han, Y. Luo, C. Sun, Z. Hao, B. Xiong, L. Wang, H. Li, Characteristics of hexagonal c-oriented titanium film as the template for GaN epitaxy on glass substrate by electron beam evaporation, Thin Solid Films 624 (2017) 160–166.

[8] G. Bernhardt, C. Silvestre, N. LeCursi, S. Moulzolf, D. Frankel, R. Lad, Performance of Zr and Ti adhesion layers for bonding of platinum metallization to sapphire substrates, Sensors and Actuators B: Chemical 77 (2001) 368–374.

[9] A. Popov, I. Pyshmintsev, S. Demakov, A. Illarionov, T. Lowe, A. Sergeyeva, R. Valiev, Structural and mechanical properties of nanocrystalleve titanium processed by severe plastic deformation, Scripta Materialia 37 (1997) 1089 – 1094.

[10] F. E. Wawner, K. R. Lawless, Epitaxial Growth of Titanium Thin Films, Journal of Vacuum Science and Technology 6 (1969) 588–590.

[11] C. Graham, M. M. M. Frances, R. A. Maniyara, Y. Wen, P. Mazumder, V. Pruneri, Nacl substrates for high temperature processing and transfer of ultrathin materials, Scientific reports 10 (2020) 1–7.

[12] J. M. Fink, M. Kalaee, A. Pitanti, R. Norte, L. Heinzle, M. Davanço, K. Srinivasan, O. Painter, Quantum electromechanics on silicon nitride nanomembranes, Nature communications 7 (2016) 1–10.

[13] J. O'Neal, R. Wyatt, F. Leonhard, The deposition of titanium on sapphire in ultrahigh vacuum, Journal of Crystal Growth 7 (1970) 177 – 178.

[14] J. Narayan, B. C. Larson, Domain epitaxy: A unified paradigm for thin film growth, Journal of Applied Physics 93 (2003) 278–285.

[15] V. P. Vlasov, A. E. Muslimov, A. V. Butashin, V. M. Kanevsky, Sapphire evolution of the vicinal (0001) sapphire surface upon annealing in air, Crystallography Reports 61 (2016) 58–62.

[16] J. W. Evans, P. A. Thiel, M. C. Bartelt, Morphological evolution during epitaxial thin film growth: Formation of 2D islands and 3D mounds, Surface Science Reports 61 (2006) 1–128.

[17] J. C. Huang, R. R. Du, C. P. Flynn, Nucleation processes in the growth of hcp titanium, Physical Review Letters 66 (1991) 341–344.

[18] R. Checchetto, Titanium thin film deposition in a deuterium atmosphere, Thin Solid Films 302 (1997) 77–83.

[19] M. J. Jung, K. H. Nam, L. R. Shaginyan, J. G. Han, Deposition of Ti thin film using the magnetron sputtering method, Thin Solid Films 435 (2003) 145–149.

[20] H. Savaloni, A. Taherizadeh, A. Zendehnam, Residual stress and structural characteristics in Ti and Cu sputtered films on glass substrates at different substrate temperatures and film thickness, Physica B: Condensed Matter 349 (2004) 44–55.

[21] T. Sonoda, A. Watazu, J. Zhu, W. Shi, K. Kato, T. Asahina, Structure and mechanical properties of pure titanium film deposited onto TiNi shape memory alloy substrate by magnetron DC sputtering, Thin Solid Films 459 (2004) 212–215.

[22] Freibertshauser Pe, McCamont Jw, Electrical properties of Titanium, Zirconium and Hafnium films from 3000K to 1.30K, J Vacuum Science & Technology 6 (1969) 184–187.

[23] G. Dehm, C. Scheu, M. Rühle, R. Raj, Growth and structure of internal cu/al2o3 and cu/ti/al2o3 interfaces, Acta Materialia 46 (1998) 759 –772.

[24] M. Huth, C. P. Flynn, Titanium thin film growth on small and large misfit substrates, Applied Physics Letters 71 (1997) 2466–2468.

[25] M. Koyama, S. Arai, S. Suenaga, M. Nakahashi, Interfacial reactions between titanium film and single crystal α-Al2O3, Journal of Materials Science 28 (1993) 830–834.

[26] G. Campbell, T. LaGrange, W. King, J. Colvin, A. Ziegler, N. Browning, H. Kleinschmidt, O. Bostanjoglo, The hcp to bcc phase transformation in ti characterized by nanosecond electron microscopy, Proceedings of an International Conference on Solid-Solid Phase Transformations in Inorganic Materials 2 (2005).

[27] L. J. Van der Paw, A method of measuring specific resistivity and hall effect of discs of arbitrary shape, in: Semiconductor Devices: Pioneering Papers, World Scientific, 1991, pp. 174–182.

[28] P. Scherrer, Bestimmung der inneren Struktur und der Größe von Kolloidteilchen mittels Röntgenstrahlen, Springer Berlin Heidelberg, Berlin, Heidelberg, 1912, pp. 387–409.

[29] The Lattice Constants of High Purity Alpha Titanium, Proceedings of the Physical Society 80 (1962) 783–786.

[30] E. Tal-Gutelmacher, R. Gemma, A. Pundt, R. Kirchheim, Hydrogen behavior in nanocrystalline titanium thin films, Acta Materialia 58 (2010) 3042–3049.

[31] E. Tal-Gutelmacher, A. Pundt, R. Kirchheim, The effect of residual hydrogen on hydrogenation behavior of titanium thin films, Scripta Materialia 62 (2010) 709–712.

[32] F. D. Enck, J. G. Dommel, Behavior of the Thermal Expansion of NaCl at Elevated Temperatures, Journal of Applied Physics 36 (1965) 839–844.

[33] J. Narayan, B. C. Larson, Domain epitaxy: A unified paradigm for thin film growth, Journal of Applied Physics 93 (2003) 278–285.

[34] J. C. Wurst, J. A. Nelson, Lineal Intercept Technique for Measuring Grain Size in Two-Phase Polycrystalline Ceramics, Journal of the American Ceramic Society 55 (1972) 109.

[35] S. Sadeghi-Khosravieh, K. Robbie, Morphology and crystal texture in tilted columnar micro-structured titanium thin film coatings, Thin Solid Films 627 (2017) 69–76.

[36] M. Vopsaroiu, G. V. Fernandez, M. J. Thwaites, J. Anguita, P. J. Grundy, K. OGrady, Deposition of polycrystalline thin films with controlled grain size, Journal of Physics D: Applied Physics 38 (2005) 490–496.

[37] J. Bae, H. Lee, D. Seo, S. Yun, J. Yang, S. Huh, H. Jeong, J. Noh, Grain size and phase transformation behavior of tini shape-memory-alloy thin film under different deposition conditions, Materials 13 (2020).

[38] J. Estel, H. Hoinkes, H. Kaarmann, H. Nahr, H. Wilsch, On the problem of water adsorption on alkali halide cleavage planes, investigated by secondary ion mass spectroscopy, Surface Science 54 (1976) 393–418.

[39] P. Cabrera-Sanfelix, A. Arnau, G. R. Darling, D. Sanchez-Portal, Water Adsorption and Diffusion on NaCl(100), The Journal of Physical Chemistry B 110 (2006) 24559–24564.

[40] C. Thompson, R. Carel, Texture development in polycrystalline thin films, Materials Science and Engineering B 32 (1995) 211–219.

[41] V. A. Moskalenko, A. R. Smirnov, A. V. Moskalenko, Cryomechanically obtained nanocrystalline titanium: microstructure and mechanical properties, Low Temperature Physics 35 (2009) 905–907.

[42] Y. Chen, D. M. Bagnall, H.-j. Koh, K.-t. Park, K. Hiraga, Z. Zhu, T. Yao, Plasma assisted molecular beam epitaxy of ZnO on c-plane sapphire: Growth and characterization, Journal of Applied Physics 84 (1998) 3912–3918.

[43] Y. Wang, S. Wang, S. Zhou, J. Xu, J. Ye, S. Gu, R. Zhang, Q. Ren, Effects of sapphire substrate annealing on ZnO epitaxial films grown by MOCVD, Applied Surface Science 253 (2006) 1745–1747.

[44] J. Brockman, M. G. Samant, K. P. Roche, S. S. P. Parkin, Substrate-induced disorder in V2O3 thin films grown on annealed c-plane sapphire substrates, Applied Physics Letters 101 (2012) 51606.

[45] T. Hayashi, A. Yamashita, T. Maruno, S. Fölsch, H. Konami, M. Hatano, In-plane ordering of a dibenzo[b,t]phthalocyaninato-zn(ii) thin film due to the atomic step arrays on a sapphire (1012) surface, Journal of Crystal Growth 156 (1995) 245 – 251.

[46] G. H. Gilmer, M. H. Grabow, Models of Thin Film Growth Modes 39 (1987) 19–23.

[47] Y. Kakehi, K. Satoh, T. Yotsuya, S. Nakao, T. Yoshimura, A. Ashida, N. Fujimura, Epitaxial growth of CuScO2 thin films on sapphire a-plane substrates by pulsed laser deposition, Journal of Applied Physics 97 (2005) 83535.

[48] D. Rasic, J. Narayan, Epitaxial growth of thin films, in: V. Glebovsky (Ed.), Crystal Growth, IntechOpen, Rijeka, 2019.

[49] D. Gall, The search for the most conductive metal for narrow interconnect lines, Journal of Applied Physics 127 (2020) 050901.

[50] M. E. Day, M. Delfino, J. A. Fair, W. Tsai, Correlation of electrical resistivity and grain size in sputtered titanium films, Thin Solid Films 254 (1995) 285–290.

[51] G. Gould, C. Grahman, E. Grünbaum, L. Moraga, J. Müller, D. C. Larson, Electrical resistivity of epitaxial titanium films, Thin Solid Films 13 (1972) 61–66.

[52] J. Caballero, G. Kremer, L. Moraga, Electrical resistivity of very thin single-crystal titanium films as a function of temperature, Thin Solid Films 117 (1984) 1–8.

[53] E. A. Bel'skaya, E. Y. Kulyamina, Electrical resistivity of titanium in the temperature range from 290 to 1800 K, High Temperature 45 (2007) 785–796.